1999 IEEE International Conference on Control Applications
Kohala Coast - Island of Hawaii, August 22-27, 1999

Bayesian Belief Networks for Fault Identification in Aircraft Gas Turbine Engines

Timothy A. Mast, Aaron T. Reed, Stephen Yurkovich†, The Ohio State University, Columbus OH
Malcolm Ashby, Shrider Adibhatla, GE Aircraft Engines, Cincinnati, Ohio

Abstract

This paper describes the methodology for usage of Bayesian Belief Networks (BBNs) in fault detection for aircraft gas turbine engines. First, the basic theory of BBNs is discussed, followed by a discussion on the application of this theory to a specific engine. In particular, the selection of faults and the means by which operating regions for the BBN system are chosen are analyzed. This methodology is then illustrated using the GE CFM56-7 turbofan engine as an example.

1. Introduction

Current methods for fault identification in aircraft gas turbine engines involve post-flight ground based trending schemes to evaluate the general fitness and condition of the engines. These trending techniques follow the historical trends of selected parameters to evaluate the condition of the engine. However, the effectiveness of these methods is dependent upon the speed with which these trending procedures can be accomplished. In the ideal case, trend data would be analyzed and faults identified following each flight. Identified faults could then be corrected prior to the next flight. The labor-intensive nature of the trending procedure prevents this from occurring and the ideal case is rarely obtained. Furthermore, even when trending data identifies a large step change in engine parameters, identification and isolation of the underlying fault is often a difficult and time consuming process.

This difficulty in fault identification is compounded by the fact that, in a complex system such as a jet engine, engine parameters are often affected by multiple systems. For example, a large increase in the specific fuel consumption of an engine could be caused by damage in any one of several parts of the engine. That is, there are no simple rules of the type "If parameter j increases by 2%, fault k is the cause." This level of uncertainty can lead to many hours of visual inspections in an effort to identify faults. The man-hours involved in such an exhaustive search are both costly and inefficient.

The advent of several new techniques in fault identification leads to a method capable of handling the associated uncertainty in these events. Some of the methods currently being investigated include use of wavelets[1], use of engine behavior models[2,3], and analysis of fault signatures using transient data[4]. The use of BBNs offers a means by which fault identification in gas turbine engines may be accomplished in a timely and efficient manner. BBNs operate by treating changes in engine outputs as random variables. These random variables can then be associated in a probabilistic sense with the underlying faults. This method allows the uncertainties inherent in the system to be absorbed into the conditional probabilities of the BBNs. Using this method, faults can be quickly identified and corrected prior to the next flight. This paper will focus on the use of BBNs to detect faults in a specific engine, the GE CFM56-7 turbofan.

†Corresponding author: yurkovich.1@osu.edu, Dept. of Electrical Engineering, The Ohio State University, 2015 Neil Avenue, Columbus, OH 43210.

2. Bayesian Belief Networks

BBNs offer a method for describing systems where causal relationships exist between events, but deterministic relationships cannot be obtained.[5,6] This is very much the situation which occurs in modern jet engines. Engine outputs are affected by many factors such as the overall health of the engine, the current operating conditions, the condition of the sensors, and the interdependencies of various subsystems. Because of the uncertainty created by these interdependent factors, it is very difficult to match a step change in output parameters with its corresponding fault. However, if the occurrence of these parameter changes are treated as random variables, the relationships between the underlying faults and the output parameter changes are described by a probabilistic relation. When handled in this manner, BBNs can offer significant advantages over traditional methods of fault isolation.

BBNs operate on the underlying principle of Bayes' Theorem. When the probability of event X occurring is written as P(X) and the conditional probability of event X occurring given that event Y has already occurred is written as P(X|Y), Bayes' Theorem can be written in the following manner:

$$P(A|B) = \frac{P(B|A)P(A)}{P(B)}$$

In this case, the event A denotes a particular fault and the event B is a step change in a certain engine output. If the conditional probabilities of the fault which causes a certain step change and the *a priori* probability of that fault occurring are known, it is possible to calculate the probability of that fault having occurred based on the occurrence of a step change in engine output. In this manner, one can identify, with some probability, the type of fault which has occurred based on the knowledge of the engine step output changes.

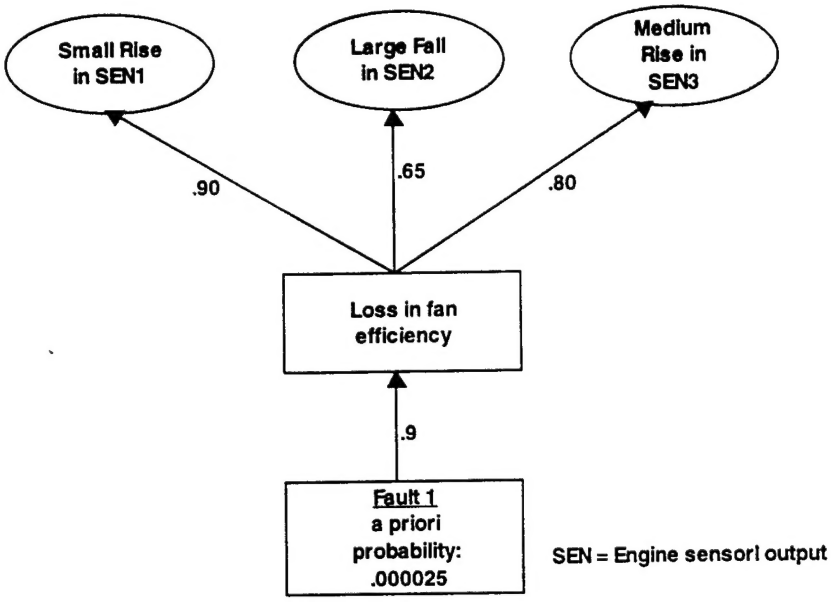

Figure 1 - Example of BBN system used for fault detection

Belief networks are actually a compact visual representation of the complete set of conditional relations between faults and their corresponding set of indicator changes. They take the form of a cause and effect mapping between root causes (faults) and the associated symptoms (indicator changes). When designing BBNs, it is important to identify the appropriate faults and indicator changes in the specific system. Next the engineer must transfer his knowledge of the system and the associated uncertainties into the conditionally probabilistic structure of the BBN. Through this process, the BBN becomes, in a sense, an expert system. However, unlike some expert systems, no learning is done.

The complete specification of a BBN network involves the identification of the probabilities associated with each event and the overall structure of the BBN. In this instance, the BBNs are of the form shown in Figure 1.

The simple example of Figure 1 illustrates one fault and the associated changes in indicator values. The root cause fault is associated with an *a priori* fault probability. This probability defines the likelihood that a certain fault will occur based upon historical field data or the engineer's knowledge of the system. The links between the nodes in the BBN are the associated conditional probabilities. In this example, with a 0.9 probability, the occurrence of fault 1 will cause a loss in fan efficiency. This type of conditional probability can be used to incorporate any type of uncertainty associated with either measurement errors or unknown engine dynamics. The specification of this conditional probability is described later.

The loss in fan efficiency then gives rise to three changes in indicator values. Likewise, these changes have conditional probabilities associated with them. Suppose, for example, that one is very confident that a loss in fan efficiency will produce a small rise in the MO1 indicator. It is therefore assigned a very high probability of 0.9. However, perhaps due to lack of confidence in the associated sensor, much less confidence is associated with the fact that a large fall in MO2 will occur. Therefore, this indicator is only assigned a probability of 0.65. It is in situations exactly such as this that BBNs prove their worth. In any type of rule-based system, a confidence level of 0.65 would be so low that it could not be used in the system. Although this indicator may not be a reliable means of indicating the fault by itself, it does contain some information that may be useful. BBNs provide a means of extracting some information from these indicators that could not be used otherwise.

In actual implementation, the uppermost level of indicators are set to Boolean TRUE and FALSE values. The BBN structure is then used to calculate the conditional probabilities associated with each fault. One can then say with some confidence level that a certain fault has occurred based upon the given set of indicator changes. Not only does the belief network provide a means of identifying the fault which has occurred, but its very structure provides a means by which one can talk about the confidence level associated with the fault identification.

3. Fault Selection

One difficulty with the use of BBNs in fault detection is that, unlike rule-based systems or neural networks, it is not possible to identify a fault for which the system has not been designed. That is, there is no "unidentified fault" classification which can be used to show that the engine is operating abnormally for reasons unknown. Moreover, BBNs possess no learning capabilities (so "training" of the system is not an issue). Therefore, care must be taken in the early

stages of the design process to identify all possible fault types that will reasonably occur.

In the example of the GE CFM56-7 engine, historical data had been used to identify the possible types of faults experienced during normal operations. The possible fault categories identified by an extensive GE survey were:

- Bird strikes and foreign object damage to fan blades
- Variable bleed valve leakage
- High pressure compressor damage
- High pressure turbine damage
- High pressure turbine clearance control valve fault
- Low pressure turbine damage
- Low pressure turbine clearance control valve fault
- Transient bleed valve fault
- CDP bleed valve leakage

In addition to these nine identified fault areas, additional faults were added to correct for the magnitude differences which could occur within a single fault category. For example, a small bird impacting the center of the fan will have a much different effect and subsequent fault signature than that arising from a large bird hitting the fan on the outer edge. To correct for these differences, magnitude levels were added in the appropriate categories (e.g. small, medium and large bird strike) to differentiate between these occurrences. This brought the total number of faults to sixteen. It is on this set of sixteen faults that all subsequent results are based. It should be noted again that, unlike a rule-based system, no data will be given for "untrained" faults. All probable faults have been accounted for in the initial building stage.

4. Operating Regions

Before discussing the actual construction of the belief networks, the operating space of the engine must first be defined. The inputs to the engine simulation make up what is referred to as the engine's operating space. This four-dimensional space defines the region over which the engine simulation can operate. The four axes of this space are altitude, mach number, throttle angle and ambient temperature. Ideally, the final fault identification scheme could correctly identify faults from any point within this space. However, the initial tests were limited to those regions where the engine will actually be operated. This reduces the complexity of the systems and allows the design to be concentrated within those areas of the space where the actual engine will be used. Based upon actual engine data, three distinct sections of the operating space were chosen for identification. The regions are defined as shown in Table 1. Notice that in the specifications in Table 1, no value is given for the ambient temperature value. During the initial design stages, the decision was made to allow the temperature to be held at that of the standard day. For all subsequent listed operating conditions, assume the ambient temperature to be that of a standard day.

Table 1: Flight regions within the operating space

Flight Phase	Altitude	Mach	Throttle Ang.
Takeoff	0 – 2000	0.22 - 0.30	68 - 78
Climb	2000 – 27000	0.30 - 0.80	72 - 74
Cruise	27000 – 39000	0.77 - 0.80	60 - 62

5. Design of BBNs for the CFM56-7

To design a BBN fault identification system for a specific application, several items must be defined. First, each fault to be identified must be determined and an *a priori* probability must be assigned to each. The *a priori* probabilities are needed to indicate the likelihood that any one problem will occur before a specific set of data is analyzed. In the context of Bayes' rule, these probabilities are the P(A) probabilities that must be known in advance to calculate the desired conditional outputs. Second, the overall structure of the BBN, defined by the indicators to be chosen, must be selected. This structure will determine the method of use for the BBN and the size of the actual working system. Finally, the conditional probabilities linking each root cause to the indicators must be determined.

In the CFM56-7 example, *a priori* probabilities for each fault were assigned based upon historical data collected over the course of a year from an engine model similar to the CFM56-7. A similar engine model was used because the CFM56-7 is a relatively new application and sufficient field data has not yet been collected. This data represents approximately 1,000,000 flight hours for the engines in question.

The standard set of sensors for this engine is comprised of two speed sensors that measure rotational speed of the engine, four temperature sensors in various locations on the engine and three pressure sensors. Of these nine standard sensors, eight proved to be useful in fault identification (the ninth, speed of the main fan, was not useful due to the fact that it was the controlled variable in the engine).

In this particular use of BBNs for fault identification, inputs to the belief network are always in the form of Boolean variables. That is, the upper level indicators are determined to be either TRUE or FALSE. To reduce the analog engine model outputs to Boolean inputs to the BBNs, magnitude levels and direction changes for each parameter were defined. For example, changes in the level of one of the model outputs were classified as small, medium, and large. In addition to these magnitude levels, directions were added to indicate whether the change was a rise or fall in the magnitude of the model output. This specific magnitude level classification created a BBN structure with 16 faults and 36 upper level indicators. In addition, there were 16 mid-level nodes which corresponded to internal changes within the engine due to each given fault. Under this scheme, any change in the levels of the model outputs of interest can be classified as a Boolean event and entered into the BBN.

With the indicator limits thus defined, it is possible to assign conditional probabilities to each of the events in the BBN. This was done by using computer simulations of the engine model and observing the effects of the faults on the model outputs in question. For example, a small bird strike was simulated using the engine model. From this simulation, it was observed that SEN1 rose. Since the amount of the SEN1 rise was directly in the center of the small rise band, the conditional probability on that indicator would be very high. For the purposes of this example, a probability of 0.95 was assigned. That is, since the value of the indicator was in the center of the magnitude band, a very high confidence level was assigned to the fact that, even with some uncertainty, the final value would still be within that band. Alternately, if the value fell near the edge of the magnitude band, a lower value of 0.6 might be chosen to show that confidence level in that indicator was not as high. If a model output value fell very near to the border between two of the magnitude bands, both adjacent indicators were given non-zero probabilities to cover the possibility that small uncertainties could place the actual value in either band. On any nonadjacent magnitude bands, the probabilities were set to zero to indicate that the actual indicator values would never vary into these bands.

These simulations were run for each of the 16 faults and values were obtained for the six model outputs in each simulation. Using this data, and the *a priori* data obtained above, a complete set of BBNs was constructed. In other words, the BBNs were completely defined by the choice of structure and the calculated probabilities.

Notice that these simulations were run at a specific point in the operating region. This point will be referred to as the "build point" of the BBN. This point can then be used to differentiate between BBNs which were designed for the same faults and the same engines, but were constructed at different points in the operating region. The reasons for this distinction will be made clear in later sections.

6. Distribution of BBNs to Cover Operating Regions

Early tests showed that these BBNs performed very well at the build points. That is, at the point in the operating regime where the BBN was designed, it could correctly identify the faults. However, the effects of faults are not constant over the entire operating region. The change in engine outputs from a fault at 35,000 feet is distinct from the change in engine outputs due to the same fault at 28,000 feet. Therefore, a single BBN designed to identify these faults at 35,000 would not be able to identify these same faults at a lower altitude. Therefore, multiple BBNs are needed to cover the areas of the operating space that are of interest. A simple scheduling algorithm can be used to switch between appropriate BBNs based on the operating condition.

7. Results for Six BBN Network

The initial testing of the BBN systems showed that fault detection was considerably easier in the cruise region as opposed to the climb and takeoff regions. For this reason, it was decided that all testing of the sensor-based BBN systems would be done on the cruise region and results, if favorable, would then be applied to the climb and takeoff regions. Early studies had shown that 2,000 ft. changes in elevation at cruise were enough to cause problems in the BBN identification system. For this reason, the cruise region was subdivided into six sub-regions (from 27,000 ft. to 39,000 ft.), where in each the mach varies between 0.75 and 0.8, and the throttle between 60 and 62. These ranges encompass the variations about the build point used by the scheduling algorithm to select the BBNs. The nominal values used as build points for each particular BBN are in the center of each of the sub-regions.

Two types of tests were performed on every complete set of BBNs. The first set of tests is referred to as the "baseline" test. In this test, the BBNs are provided with the data with which they have been built. That is, they are excited with the same data for which they have been designed. This test is done for two reasons. The first is to provide a secondary check to be sure that no input mistakes were made during the design process. The second, and more important reason, is to check how well the BBN operates with data for which it has been built. The rational is that if the BBN is unable to correctly identify a fault at the build point for which it is designed, it will not be able to identify this fault at an operating point away from the build point.

The second type of test for each BBN is referred to as the "envelope" test. In this test, the BBN is tested with data from random operating points within the variations given above. This test is intended to test how well the BBNs perform when perturbed away from the build points. It is intended as a simulation of how well the system will perform in actual use where it is highly improbable that the engine will fly exactly through the build point.

In the six BBN system, the baseline results over all seven regions are as shown in Table 2. In these results, a correct identification occurs when the BBN indicates that at least one fault has occurred with a probability of greater than 0.85. In that case, correct identification implies that the system returns the result $P(A|B)>0.85$. A correct isolation result occurs when only the correct fault is indicated.

Table 2: Six BBN system baseline test results

Performance Measure	Percentage
Correct Identification	97.92%
Correct Isolation	97.92%
Incorrect Identification	2.08%
No Identification	2.08%

These results show that the six BBNs worked quite well at the points at which they have been designed. This is not a

surprising result, but it is necessary to establish that the BBNs are performing as they should.

Following a successful baseline test, the next step is to perform an envelope test to determine how well the BBNs operate within their given region. In this test, random operating points from within the available region are chosen for testing purposes. The six BBN envelope test results are given in Table 3.

Table 3: Envelope test results for six cruise sub-regions

	Correct Identification	Correct Isolation	Incorrect Identification	No Identification
CR1	82.6%	59.2%	9.9%	7.5%
CR2	71.8%	51.5%	14.0%	14.3%
CR3	70.5%	35.3%	19.1%	10.4%
CR4	79.6%	47.0%	13.6%	6.9%
CR5	81.0%	58.4%	13.7%	5.3%
CR6	85.1%	46.3%	9.3%	5.6%
Total	78.4%	49.6%	13.3%	8.3%

Based upon the results of dividing the cruise region into six sub-regions, it is apparent that the system is not achieving the desired performance results. Since the baseline results were quite good, it is certain that the error is not coming from some design flaw in the BBNs. Therefore, the error must be coming from the variation in engine outputs due to changes in operating conditions. As these changes are not part of the designed system, the only way to compensate for these variations is to decrease the size of the regions that each individual BBN must cover. This reduction in the size of the region around the build point makes it necessary to increase the number of BBNs to maintain the coverage of the operating regions.

7. Results for 24 BBN Cruise Network

Based upon the results of the six BBN system, the next step was to determine the number of BBNs needed to increase the performance to an acceptable level. To decide how many sub-regions were needed for good performance, some correlation studies were performed. In these studies, a single fault was introduced into the engine model. This model was then flown at random operating points within the regions being studied. This test was then performed for each of the 16 faults in the test set. The results of these simulations were tested for correlation in each of the model outputs using MATLAB. The goal of these correlation studies was to show how strongly each output sensor was correlated to the operating condition. If the output sensors were only weakly correlated to operating condition within a region, then only a single BBN would be needed to cover this region as the fault signature would stay relatively unchanged. However, in the case of strong correlation, the size of the BBN operating region would need to be reduced.

The correlation results were used to identify that the sensors in use are most strongly correlated to altitude. It was for this reason that the cruise region was divided into six distinct altitude blocks. However, the correlation results also showed that the sensors were somewhat correlated to the throttle setting of the engine as well as the mach value. The original hope was that these correlations would not be strong enough to effect the final results. However, it is apparent from the results of the six sub-region system that the correlations are large enough to have an effect. To account for one of these correlations, additional sub-regions were added to split the throttle angle axis into two divisions. This created 12 sub-regions in cruise. However, results for this system were also not favorable. Therefore, an additional division in the mach axis was added to increase the number of regions to 24. Baseline results for this new system were similar to those for six sub-regions. Envelope test results are given by individual fault rather than region in Table 4.

Table 4 – Envelope test results for 24 cruise sub-regions

Fault	Correct Identification	Correct Isolation	Incorrect Identification	No Identification
1	99.96%	49.33%	0.04%	0.00%
2	100.00%	68.71%	0.00%	0.00%
3	100.00%	79.67%	0.00%	0.00%
4	24.84%	10.71%	30.13%	45.04%
5	99.87%	76.46%	0.17%	0.00%
6	82.04%	25.58%	13.58%	4.38%
7	100%	61.83%	0.00%	0.00%
8	72.88%	27.38%	25.17%	1.96%
9	87.05%	80.63%	2.79%	10.17%
10	73.38%	64.63%	2.88%	23.75%
11	21.37%	16.04%	14.04%	64.58%
12	65.66%	65.58%	15.71%	18.63%
13	95.17%	75.38%	4.33%	0.50%
14	97.33%	86.79%	2.50%	0.17%
15	84.96%	74.88%	7.71%	7.33%
16	94.63%	69.92%	4.79%	0.58%

From these results, the decision was made to create no further sub-regions within the cruise region. By analyzing the results in Table 4, it is apparent that the majority of the errors are introduced by only a few of the faults. The majority of the faults are identified with very few errors. However, the poor results over some of the faults skew the results downward.

To further refine the degree to which distinction could be brought out of the results, the faults were divided into three groups. The first group of faults are those faults for which identification was performed very well. This group includes the nine faults for which the BBN system performed the best, that is, faults in the set [1, 2, 3, 5, 7, 9, 13, 14, 16]. The second group of faults are those faults for which identification was fair but not as good as the faults in Group 1. The four faults in Group 2 are [6, 8, 10, 15]. The final group, the set [4, 11, 12], includes the three faults over which the BBNs performed very poorly. These three faults introduced 62% of the error for the total system. By

separating these faults out, the overall results are much better. The results for these groups are shown in Table 5.

Table 5 -Envelope test results for 24 sub-regions by group

Group	Correct Identification	Correct Isolation	Incorrect Identification	No Identification
1	97.11%	72.08%	1.63%	1.27%
2	78.31%	48.11%	12.33%	9.35%
3	37.29%	30.78%	19.96%	42.75%

8. Engine Deterioration Studies

All results reported to this point have been for a hypothetical ideal engine directly off the assembly line. In real world operations, an engine will not remain in this state. In fact, it is more likely that the engine in which a fault occurs will be one which has been in service for some length of time. Even new engines off the assembly line will have some small variation from the specifications because of the imperfections in the manufacturing process. Therefore, the next step would be to examine the effects of these variations on the BBN system.

Deterioration levels were obtained from GE to represent the worst levels of deterioration possible in an actual working engine. Any engine which has deteriorated below these levels would be taken out of operation to be rebuilt or retired. Simulations were run of these deteriorated engines and the results were fed through the 24 BBN system designed above. The results are given in Tables 6 and 7.

Table 6 – Deteriorated engine envelope results

Fault	Correct Identification	Correct Isolation	Incorrect Identification	No Identification
1	99.96%	43.75%	0.04%	0.00%
2	100.00%	59.46%	0.00%	0.00%
3	100.00%	69.67%	0.00%	0.00%
4	22.13%	7.33%	30.42%	47.46%
5	99.88%	63.04%	0.13%	0.00%
6	83.33%	24.00%	15.29%	1.38%
7	100.00%	45.96%	0.00%	0.00%
8	67.29%	16.79%	31.75%	0.96%
9	78.38%	76.88%	4.50%	17.13%
10	83.38%	65.29%	14.54%	2.08%
11	19.17%	15.00%	12.79%	68.04%
12	25.50%	22.96%	13.54%	60.96%
13	93.58%	77.63%	6.33%	0.08%
14	80.75%	75.21%	18.17%	1.08%
15	75.38%	58.67%	16.83%	7.79%
16	88.00%	57.08%	9.46%	2.54%

It might be expected that the results for these deteriorated engines would be appreciably worse than those for non-deteriorated engines. Surprisingly, the results for the cruise region are only slightly reduced from those for non-deteriorated engines. This result increases the confidence in a fault identification regardless of the level of deterioration.

Table 7 – Deteriorated engine envelope results by group

Group	Correct Identification	Correct Isolation	Incorrect Identification	No Identification
1	93.39%	63.19%	4.29%	2.31%
2	77.34%	41.19%	19.60%	3.05%
3	22.26%	15.10%	18.92%	58.82%

9. Conclusion

This work has shown that BBN systems can be used for fault identification in jet turbine aircraft engines. By careful scheduling of individual BBNs across the operating space, a reasonably high level of accuracy can be obtained. The limiting factor is the number of BBNs the user is willing to use to obtain a desired level of accuracy.

Since the system of BBNs designed for non-deteriorated engines performed well in the presence of deterioration, reasonable confidence can be placed in a fault identification from the system. In addition, if a moderate level of deterioration is used for the design point of the BBN network, then the system will represent a more typical engine in service and the results will be between those shown for non-deteriorated and deteriorated engines.

References

[1]N. Aretakis, K. Mathioudakis, "Wavelet Analysis for Gas Turbine Fault Diagnostics", *Journal of Engineering for Gas Turbines and Power Transactions of the ASME*, 119:(4)870-876, October 1997.

[2]L. TraveMassuyes, R. Milne, "Diagnosis of Dynamic Systems Based on Explicit and Implicit Behavioral Models: An Application to Gas Turbine Engines in Esprit Project Tiger", *Applied Artificial Intelligence*, 10:(3)257-277, May-June 1996.

[3]G.L. Merrington, "Fault Diagnosis in Gas Turbines Using a Model-Based Technique", *Journal of Engineering for Gas Turbines and Power Transactions of the ASME*, 116:(2)374-380, April 1994.

[4]R.W. Eustace, B.A. Woodyatt, G.L.Merrington, A. Runacres, "Fault Signatures Obtained from Fault Implant Tests on an F404 Engine", *Journal of Engineering for Gas Turbines and Power Transactions of the ASME*, 116:(1)178-183, January 1994.

[5]J. Pearl, *Probabilistic Reasoning in Intelligent Systems: Networks of Plausible Inference*. Morgan Kaufmann, San Mateo, CA, 1998.

[6]E. Neapolitan, *Probabilistic Reasoning in Expert Systems: Theory and Algorithms*. John Wiley and Sons, New York, 1990.

EE 753.01

Idle Speed and Air/Fuel Ratio Control;

Ford 4.6L V8 Engine

Submitted to: Professor S. Yurkovich

Aaron T. Reed and Richard J. Thomas

March 19, 1999

I. Abstract

This project considers the combined controller design challenge of Idle-Speed Control (ISC) and Air Fuel Ratio (AFR) Control through State Feedback Control (SFC) and Sliding Mode Control (SMC), respectively. The mathematical engine model is a three input, two output nonlinear event-based representation of a 4.6L Ford V8 engine. The analysis and design is conducted in the continuous crank angle domain. The plant inputs are air mass flow rate, spark advance, and injected fuel mass flow rate. The plant outputs are engine speed and measured equivalence ratio.

II. Literature Review

The first challenge in most control problems is to describe the appropriate physical phenomena with mathematical models that are accurate enough to give the control scheme a good platform upon which to achieve the desired objectives. Most of the inertial, air, fuel, and mixture dynamics discussed in this paper are thoroughly analyzed in [3]. Likewise, most of the state-variable linear control techniques applied to this problem are found in [2]. The fundamental AFR principles and challenges discussed in [1] are helpful in understanding typical control techniques applied to this tracking problem. Especially when applied directly to a nonlinear model, SMC has very good disturbance rejection properties. This paper focuses on using SMC to reject tip-in and tip-out disturbances for the AFR created by the SFC inputs that are intended to reject a 15 Nm load torque disturbance in the ISC problem. Fortunately, much of the required SMC design methodology and theory is found in [4],[5],[6].

III. Modeling and Design Methods

A. *Non-Linear Model Equations*

The engine dynamics are represented by the following non-linear continuous time equations.

$$\dot{dp_m} + \frac{\eta_v V_d}{4\pi V_m}\omega p_m = \frac{RT_m}{V_m}\dot{m}_{a,th} \tag{1}$$

$$\dot{m}_{ac} = \frac{\eta_v V_d}{4\pi RT_m}\omega p_m \tag{2}$$

$$J\frac{d\omega}{dt} + B\omega = \tau \tag{3}$$

$$\tau_i = K_\tau p_m(t - t_\tau) + K_\delta \delta \tag{4}$$

$$\frac{d\dot{m}_{ff}}{dt} = \frac{1}{\tau_f}(-\dot{m}_{ff} + X\dot{m}_{fi}) \tag{5}$$

$$\dot{m}_{fv} = (1 - X)\dot{m}_{fi} \tag{6}$$

$$\dot{m}_{fc} = \dot{m}_{fv} + \dot{m}_{ff} \tag{7}$$

$$\phi_i = \left(\frac{A}{F}\right)_s \frac{\dot{m}_{fc}}{\dot{m}_{ac}} \tag{8}$$

$$\tau_m \frac{d\phi_m}{dt} + \phi_m = \phi_i(t - t_d) \tag{9}$$

$$\phi_m = \phi_e(t - t_t) \tag{10}$$

$$\phi_e = \phi_i(t - t_c) \tag{11}$$

where
η_v is volumetric efficiency
p_m is manifold pressure in N/m^2
V_d is engine displacement volume in m^3
V_m is manifold volume in m^3
R is the air gas constant
T_m is the manifold air temperature in K
$\dot{m}_{a,th}$ is mass air flow rate through the trottle in kg/sec
ω is engine speed in rad/sec
$\dot{m}_{ac}$ is mass air flow rate to the engine cylinders
J is the total inertia of the engine and loads
B is the coefficient of damping friction
τ_i is indicated torque
t_τ is the torque delay involved in the combustion process
δ is the spark advance in degrees
K_δ converts spark advance into a spark influence torque
m_{ff} is mass of fuel evaporating from the fuel film
m_{fc} is mass of fuel entering engine cylinders
m_{fv} is mass of fuel vaporized directly into cylinders
m_{fi} is mass of fuel injected
τ_f is the fuel evaporation time constant
X is the percentage of injected fuel entering the fuel film
ϕ_i is the equivalence ratio of the inducted mixture
ϕ_e is the equivalence ratio at the exhaust valve
ϕ_m is the equivalence ratio measured by (UEGO) sensor
τ_m is the (UEGO) sensor time constant
t_c is the cycle delay
t_t is the transport delay from the exhaust valve to the (UEGO) sensor
t_d is the total delay ($t_d = t_c + t_t$)

Because many of the system delays inherent to the internal combustion engine are directly associated with the engine cycles, it is more natural to use an event-based method to model the dynamic equations. Therefore, the time-domain equations are transformed to the crank angle domain. These nonlinear equations are used to model the engine during the AFR SMC design and for testing of the combined AFR and ISC scheme.

$$\frac{dp_m}{d\theta} + \frac{\eta_v V_d}{4\pi V_m} p_m = \frac{RT_m}{V_m} \frac{dm_{a,th}}{d\theta} \tag{12}$$

$$\frac{dm_{ac}}{d\theta} = \frac{\eta_v V_d}{4\pi RT_m} p_m \tag{13}$$

$$J\frac{d\omega}{d\theta}\omega + B\omega = \tau \tag{14}$$

$$\tau_i = K_\tau p_m(\theta - \theta_\tau) + K_\delta \delta \tag{15}$$

$$\frac{d^2 m_{ff}}{d\theta^2}\omega = \frac{1}{\tau_f}\left(-\frac{dm_{ff}}{d\theta} + X\frac{dm_{fi}}{d\theta}\right) \tag{16}$$

$$\frac{dm_{fc}}{d\theta} = (1 - X)\frac{dm_{fi}}{d\theta} + \frac{dm_{ff}}{d\theta} \tag{17}$$

$$\phi_i \frac{\eta_v V_d}{4\pi R T_m} p_m = \left(\frac{A}{F}\right)_s \frac{dm_{fc}}{d\theta} \tag{18}$$

$$\tau_m \frac{d\phi_m}{d\theta}\omega + \phi_m = \phi_i(\theta - \theta_d) \tag{19}$$

B. Open Loop Analysis

The linearized system equations contain many nominal constant values. These nominal constants are determined through an open loop simulation of the non-linear theta-domain engine model. The spark advance is set to zero. The fuel mass flow input is calculated to be the air mass flow multiplied by $(F/A)_s$. This assures a stoichiometric input mixture. Next, the air mass flow is set to a constant and the resulting steady-state engine rpm is observed. This air mass flow constant is then calibrated by trial and error until a steady-state engine rpm of 740 rpm is achieved. Finally, the desired nominal constants are determined from the final simulation having a 740 rpm steady-state.

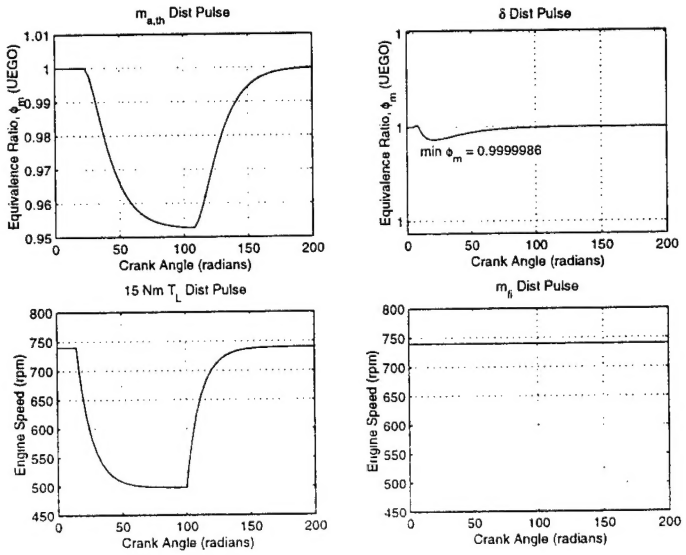

Figure 1: Open loop pulse disturbance tests

Open loop tests are performed to assess the influence of the ISC inputs (air mass flow and spark advance) on the AFR output and the influence of the AFR control input (fuel mass flow) on the idle speed. This is a special point of interest since the proposed ISC and AFR control are autonomous

with repect to each other. As shown in Figure (1), if a 5% from nominal air mass flow pulse disturbance input is applied, then the equivalence ratio ϕ_m decreases to approximately 0.952. Similarly, if a 5 degree spark advance pulse disturbance is applied, then ϕ_m remains virtually unchanged as shown in Figure (1). For a $15Nm$ torque load pulse disturbance, the engine speed decreases significantly to 500 rpm as shown in Figure (1). The engine rpm remains virtually unchanged when a 5% from nominal fuel mass flow pulse disturbance is introduced as shown in Figure (1).

C. Non-Linear Air/Fuel Ratio Control

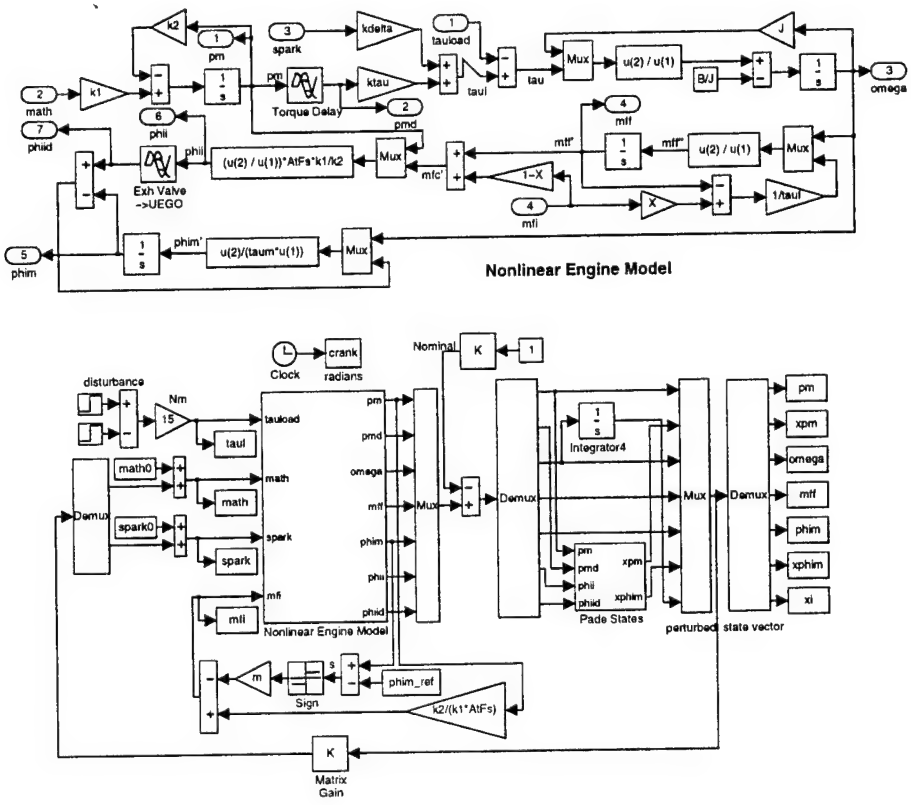

Figure 2: The non-linear engine model with ISC and AFR control.

First, the non-linear time equations (1) through (11) are reformulated to yield eight non-linear continuous crank angle domain equations (12) through (19). Next, open loop pulse input tests are conducted to observe open loop response and to establish constants corresponding to nominal values.

Evaluating the results of the open loop AFR ϕ_m response, one can see that the equivalence ratio dropped by almost 5%, whereas the goal is to keep ϕ_m within 0.5% of ϕ_{ref} in order to maximize the efficiency of the catalytic converter. To further increase the efficiency of the catalytic converter, it is desired to have the AFR oscillate between lean and rich. Therefore, because of this inherent feature and because the fuel and mixture dynamics are nonlinear, a sliding-mode controller is used to achieve the performance specifications for the AFR portion of the problem.

There are two items that need to be selected for the basic sliding-mode controller design, the sliding surface S and the gain m. Depending on which side of the line the present output value resides, the sliding surface acts as a switching line to decide which of two control actions to implement. In this case, it is desired to track a reference equivalence ratio. Therefore the following sliding surface

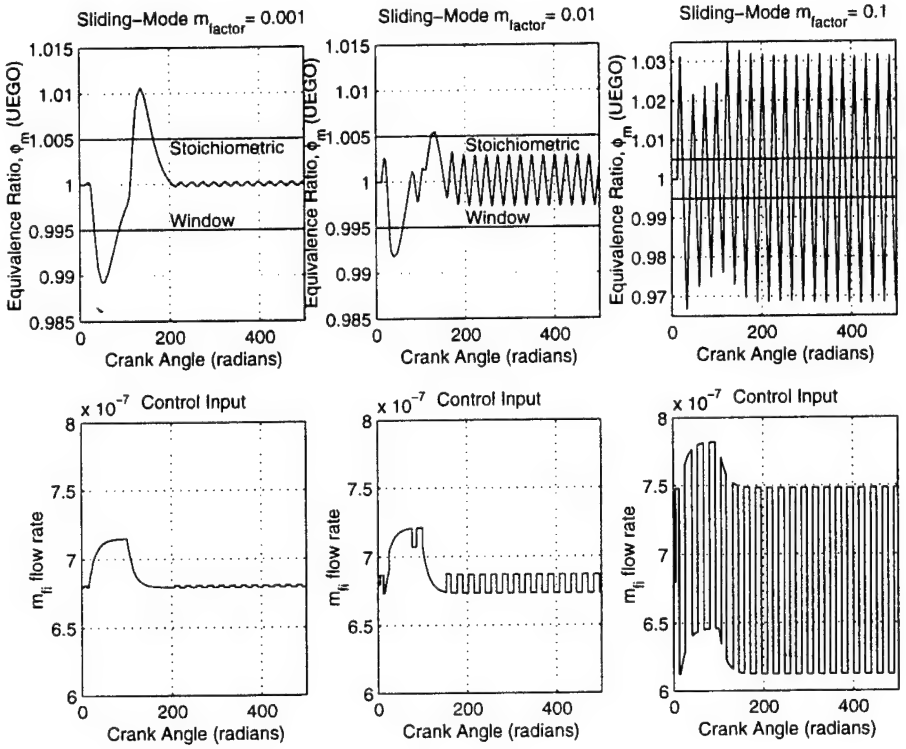

Figure 3: SMC gain comparison.

is defined.

$$S = \phi_m - \phi_{ref} \tag{20}$$

Notice that if $\phi_m > \phi_{ref}$, then $S > 0$; if $\phi_m < \phi_{ref}$, then $S < 0$. Once it is determined that the measured output is above or below the chosen boundary, this positive or negative value is input into the signum function. Thus, plus or minus one is multiplied by the gain m to establish the value of the feedback portion of the control input. The gain establishes the speed of the response back to the desired reference. The higher the gain, the more significance the controller places on the decision that the measured output is away from the desired reference. This positive or negative gain term is then subtracted from the feedforward portion of the control. In this situation, since the control input for the AFR control is $\dot{m}_{fi}$, this feedforward term functions as a nominal $\dot{m}_{fi}$ to be added. The gain term adds knowledge of the output to the control by adding or subtracting the gain from the nominal $\dot{m}_{fi}$. The following equation is the total sliding-mode control input.

$$u = \frac{\frac{dm_{ac}}{d\theta}}{\left(\frac{A}{F}\right)_s} - msign\,(S) \tag{21}$$

To understand the effects of equation (21), evaluate a simple case. If the AFR mixture is rich, (i.e. $\phi_m > 1$) then $S > 0$ and less than nominal fuel is injected into the cylinder as a result of the control. To determine the proper controller gain, various m-values are selected and their effects are compared. Because the feedback term is subtracted from the nominal feedforward term m is calculated using the following method.

$$m = m_{factor}\dot{m}_{fc_o} \tag{22}$$

Figure (3) shows the results of three different m-values implemented, $m \in \{0.001, 0.01, 0.1\}$, using $\dot{m}_{fi}$ to control ϕ_m, which is one of the ouputs of the nonlinear engine model experiencing $\dot{m}_{a,th}$ and spark pulse disturbances. The following equations explain why as m_{factor} increases the response of ϕ_m is faster and has a higher bound on its limit cycle behavior.

$$u \cong \dot{m}_{fc_o} - msign(S) \tag{23}$$

$$u \cong \dot{m}_{fc_o}\alpha \tag{24}$$

Because the control is directly proportional to $\alpha = (1 \pm m_{factor})$, the higher the m_{factor}, the more violent the control input becomes. An $m_{factor} = 0.01$ is chosen to strike a balance between the speed of the AFR response and the bound on the oscillations about stoichiometry. The nonlinear engine model used in the design of the SMC is shown in Figure (2). Also in Figure (2) is the diagram of the SMC which uses states from the nonlinear subsystem to control ϕ_m with $\dot{m}_{fi}$. (This diagram also represents the full integration of both the SMC and the SFC. This integration is discussed later).

D. Linearized Model Equations

The linearized perturbation crank angle domain equations (25) through (30) are derived from equations (12) through (19). These equations are used to model the engine during the state feedback ISC design.

$$\frac{dp_m}{d\theta} + \frac{\eta_v V_d}{4\pi V_m} p_m = \frac{RT_m}{V_m}\frac{dm_{a,th}}{d\theta} \tag{25}$$

$$\frac{d\omega}{d\theta} = \frac{1}{J\omega_0}\tau - \frac{\tau_0}{J\omega_0^2}\omega \tag{26}$$

$$\tau_i = K_\tau p_m(\theta - \theta_\tau) + K_\delta \delta \tag{27}$$

$$\omega_0 \frac{d^2 m_{ff}}{d\theta^2} + m_{ff0}\omega = \frac{1}{\tau_f}\left(-\frac{dm_{ff}}{d\theta} + X\frac{dm_{fi}}{d\theta}\right) \tag{28}$$

$$\phi_i \frac{\eta_v V_d}{4\pi R T_m} = \left(\frac{A}{F}\right)_s \left(\frac{1}{p_{m0}}\left((1-X)\frac{dm_{fi}}{d\theta} + \frac{dm_{ff}}{d\theta}\right) - \frac{m_{fc0}}{p_{m0}^2} p_m\right) \tag{29}$$

$$\phi_m = \phi_i(\theta - \theta_d) - \tau_m\left(\omega_0 \frac{d\phi_m}{d\theta} + \phi_{m0}\omega\right) \tag{30}$$

E. Linear Idle Speed Control

The first step for the design of state feedback control for ISC is the approximation of the two system delays θ_τ and θ_d. These are approximated by first order *Padé* approximations.

$$P_d(s) = \frac{1 - \frac{s\theta_d}{2}}{1 - \frac{s\theta_d}{2}} \tag{31}$$

where $P_d(s)$ and T_d are the transfer function and the approximated delay, respectively. The corresponding state space equations are

$$\frac{dx}{d\theta} = -\frac{2}{\theta_d}x + u = Ax + Bu \tag{32}$$

$$y = \frac{4}{\theta_d}x - u = Cx + Du \tag{33}$$

An approximation of the ficticious state within the Simulink transport delay block can be obtained by solving for the state variable x in equation (33) thus yielding

$$x = \frac{\theta_d}{4}(y + u) = \frac{1}{C}(y - Du). \tag{34}$$

Hence, this state can be obtained for simulation purposes by connections at the input u and output of the delay block y (e.g. p_m and $p_m(\theta - \theta_d)$). The two derived states are then combined with the original four system states for state feedback control.

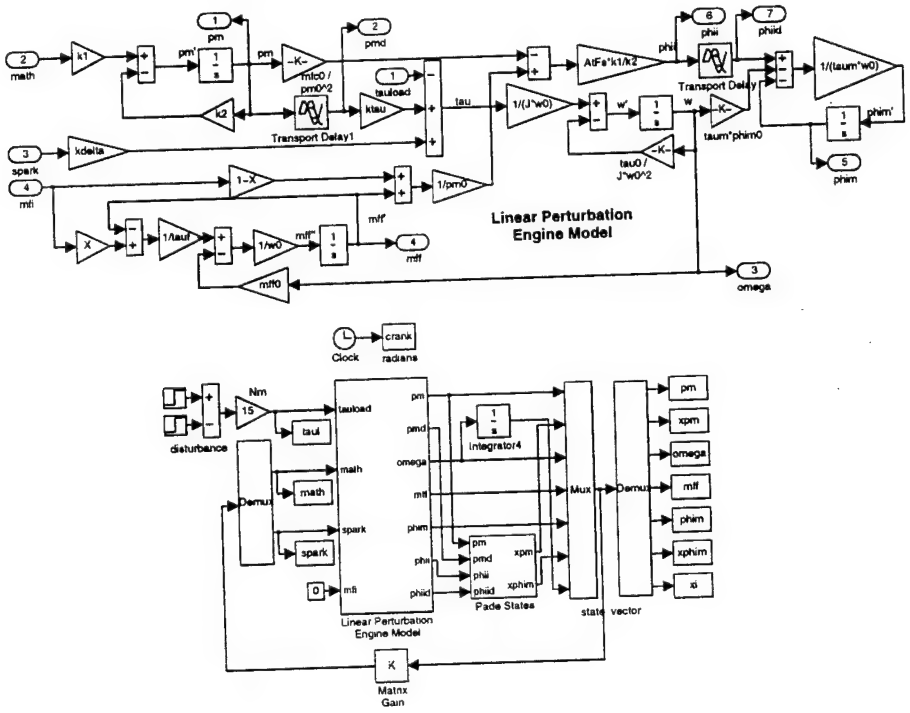

Figure 4: The linear perturbation model with state feedback control (shown with integral action).

The linear perturbation model with state feedback control is shown in Figure (4). The state feedback matrix for SFC without integration action is determined through pole placement. The initial determination of the poles is based on a previous ISC controller design for this plant. The final pole selection is

$$s_{1,2} = -0.4012 \pm 0.0834i \quad s_5 = -2.1988$$
$$s_{3,4} = -0.2485 \pm 0.1218i \quad s_6 = -3.2982$$

from which the following controller gain matrix is obtained through the use of the 'place' command in Matlab.

$$K_{2x6} = \begin{bmatrix} 5.338e-05 & 1.421e-05 & -9.778e-06 & 1.354e+03 & -3.007e-04 & -8.351e-05 \\ -8.7149 & -7.5047 & 9.6236 & -7.972e+08 & 97.9018 & 15.0666 \end{bmatrix}$$

The simulation of the closed loop system response with this controller is shown in the top row of plots in Figure (5). The maximum excursion and steady-state error are approximately 7 rpm and 2 rpm, respectively.

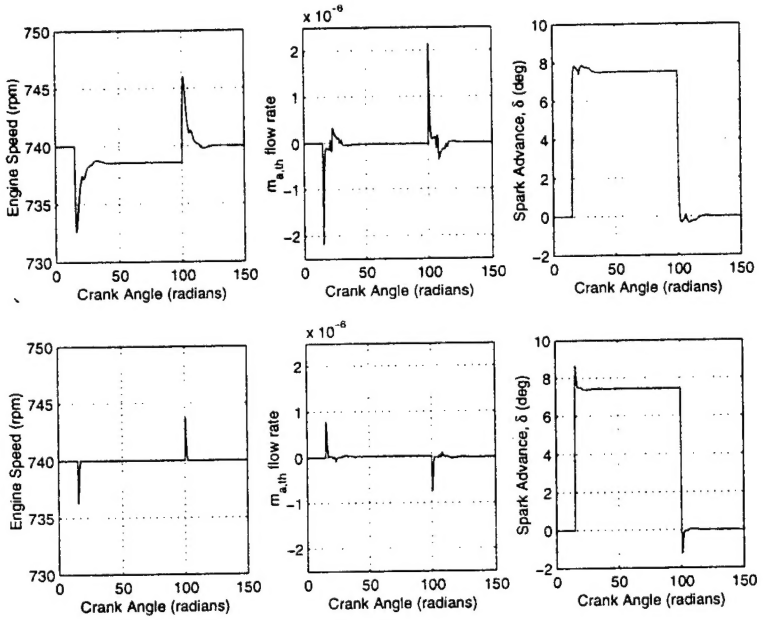

Figure 5: SFC Simulation. Top: without integrator. Bottom: with integrator.

Next, the state feedback design is modified to include integral action to eliminate steady-state error as shown in Figure (4). The six states are augmented with a seventh state and $s_i = -0.5749$ is selected as the seventh pole. The following gain matrix is obtained from the Matlab 'place' command.

$$K_{2x7} = \begin{bmatrix} 6.45e-05 & 6.85e-06 & 1.87e-06 & 1.53e+03 & -4.68e-04 & -1.71e-04 & 1.23e-05 \\ -3.0279 & 2.1480 & 12.7418 & 1.19e+08 & 9.2536 & 3.4667 & 18.8791 \end{bmatrix}$$

The simulation of the closed loop system response with this controller is shown in the bottom row of plots in Figure (5). The maximum excursion and steady-state error are approximately 4 rpm and 0 rpm, respectively.

IV. Results

Interestingly, even though the nonlinear AFR controller and the linear ISC controller are designed separately, they are simultaneously incorporated around the nonlinear engine model with virtually no changes to either controller. The only implementation consideration is that the SFC is designed with a linearized perturbation model. Therefore, before the states are used for feedback, the nominal state values are subtracted from the nonlinear model states. Then, before the SFC control inputs are sent into the model, the perturbation control vector is added to a nominal input vector. This procedure is seen clearly in Figure (2).

The results of the combined AFR/ISC controller, as shown in Figure (6), are quite good. The control clearly rejects the torque load disturbance while maintaining the AFR within 0.5% of stoichiometry. As expected, most of the ISC control is achieved through spark advance. In addition, the AFR control performed well while experiencing tip-in and tip-out disturbances caused by the ISC control inputs. After seeing the results of the open-loop disturbance tests. where the spark advance disturbance has very little effect on AFR control, one can predict these well-behaved responses.

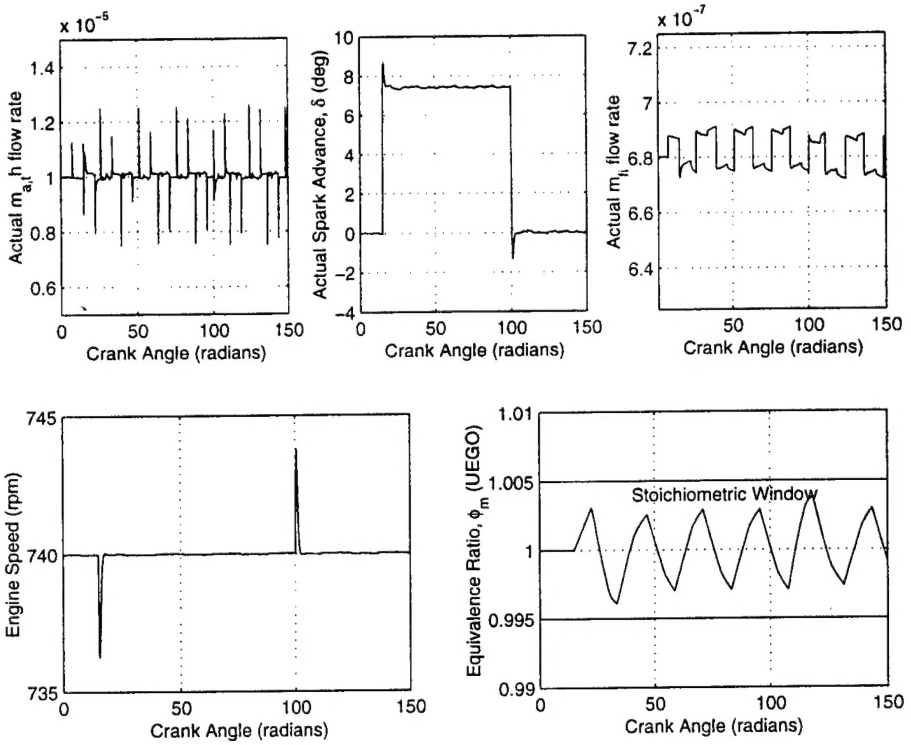

Figure 6: Final simulation results. Top: inputs. Bottom: outputs.

The most interesting result is that the $\dot{m}_{a,th}$ input has so many spikes. This phenomenom is a direct result of the SMC purposely introducing rapid oscillations about $\phi_m = 1$. These oscillations introduce oscillations in many of the states, which are in turn, multiplied by a gain matrix. Because the spikes are not as noticeable in the spark advance input, it appears that the gain vector associated with the spark advance is smaller, on a percentage basis, than the gain vector associated with the $\dot{m}_{a,th}$. It can be shown that as the gain in the SMC is reduced, the oscillations in AFR become slower and smoother, which in turn greatly reduces the spikes in the $\dot{m}_{a,th}$ input. Thus, there is a trade-off between fast AFR control and smooth $\dot{m}_{a,th}$ for ISC control. Supposing that the idle-bypass valve is a low pass filter, one would expect minimal operational problems due to the spikes. Therefore, the oscillations created by the SMC are beneficialsince they promote catalytic converter efficiency.

V. Conclusion

Since the plant is inherently event-based, the engine model is first converted to the crank angle domain. Secondly, an open-loop analysis of the plant model is performed. Next, SMC is designed to track a reference AFR. Then, ISC is achieved by state feedback control with integral action. Finally, the two controllers are implemented and tested on the non-linear plant model.

Analysis of air mass flow and fuel mass flow units reveals that there exists some inconsistencies with respect to constants in the equations. Specifically, the ratio of $\dot{m}_{a,th_0}$ to $\dot{m}_{fi_0}$ does not correspond to expected values for air-to-fuel ratio. Additional information with respect to units could lead to a resolution of this issue. Equations (1), (12), and (25) are considered the most probable sources of the apparent disparity since they contain $\dot{m}_{a,th_0}$.

Simulations provide interesting insights into the dynamics relating the inputs to the outputs. For example, the ISC air mass flow input significantly affects the measured equivalence ratio. In addition, the spark advance and fuel mass flow inputs have virtually no affect on the equivalence ratio and the engine idle speed, respectively. A 15 Nm torque load disturbance considerably alters steady-state engine idle speed. In addition to the above effects, state oscillations occur when the AFR SMC is implemented. Analysis of the simulink diagram and consideration of the dynamical equations confirm the simulation results.

This study of the impact of combining ISC with AFR control suggests future directions of study. Although all design methods and simulation results within this paper are based on the assumption that all states are available for feedback, observer based state feedback would be a viable method since the system structure is observable. A potential modification of the controller proposed within this paper would be to zero the gains of the artificial states, thus effectively reducing the system dimension to four. Comparison of this modified design with a design approach that ignores the system delays throughout the design procedure would be intriguing. Another direction for future study would be to attempt to accomplish design specifications assuming greater restrictions on the spark advance input. Finally, all of these previous approaches could be evaluated while using a non-linear AFR sensor.

VI. References

[1] Chang, C., N. P. Fekete, A. Amstutz, J. D. Powell, "Air-Fuel Ratio Control in Spark-Ignition Engines Using Estimation Theory," *IEEE Transactions on Control Systems Technology, Vol. 3, No. 1, March 1995*

[2] Franklin, G. F., J. D. Powell, M. Workman, *Digital Control of Dynamic Systems 3rd ed.*, Addison Wesley Longman, 1998

[3] Rizzoni, G., K. C. Srinivasan, *Mechanical Engineering 781 Powertain Dynamics*, The Ohio State University Department of Mechanical Engineering, 1998

[4] Utkin, V. I., "Sliding Mode Control Design Principles and Applications to Electric Drives," *IEEE Transactions on Industrial Electronics, Vol. 40, No. 1, February 1993*

[5] Utkin, V. I., Course Materials for Prof. Utkin's Autumn 1999 EE 859 control course (which includes Sliding Mode Control)

[6] Utkin, V. I., *Sliding Modes in Control and Optimization*, Springer-Verlag, 1992

REPORT DOCUMENTATION PAGE	Form Approved OMB No. 0704-0188

1. AGENCY USE ONLY *(Leave blank)*	2. REPORT DATE	3. REPORT TYPE AND DATES COVERED
	15.Jun.00	MAJOR REPORT

4. TITLE AND SUBTITLE
BAYESIAN BELIEF NETWORKS FOR FAULT IDENTIFICATION IN AIRCRAFT GAS TURBINES

5. FUNDING NUMBERS

6. AUTHOR(S)
CAPT REED AARON T

7. PERFORMING ORGANIZATION NAME(S) AND ADDRESS(ES)
OHIO STATE UNIVERSITY

8. PERFORMING ORGANIZATION REPORT NUMBER

9. SPONSORING/MONITORING AGENCY NAME(S) AND ADDRESS(ES)
THE DEPARTMENT OF THE AIR FORCE
AFIT/CIA, BLDG 125
2950 P STREET
WPAFB OH 45433

10. SPONSORING/MONITORING AGENCY REPORT NUMBER
FY00-217

11. SUPPLEMENTARY NOTES

12a. DISTRIBUTION AVAILABILITY STATEMENT
Unlimited distribution
In Accordance With AFI 35-205/AFIT Sup 1

12b. DISTRIBUTION CODE

13. ABSTRACT *(Maximum 200 words)*

DISTRIBUTION STATEMENT A
Approved for Public Release
Distribution Unlimited

14. SUBJECT TERMS	15. NUMBER OF PAGES 10
	16. PRICE CODE

17. SECURITY CLASSIFICATION OF REPORT	18. SECURITY CLASSIFICATION OF THIS PAGE	19. SECURITY CLASSIFICATION OF ABSTRACT	20. LIMITATION OF ABSTRACT